High Precision Control for Twin-Drive System Based on Mode Decoupling with Virtual Viscosity: Equivalent Controller Transform for Machine Tool

Kota Fujimoto[1], Hiroshi Fujimoto[2]
The University of Tokyo
Kashiwa, Chiba, Japan
fujimoto.kota21@ae.k.u-tokyo.ac.jp[1], fujimoto@k.u-tokyo.ac.jp[2]

Yoshihiro Isaoka[3], Yuki Terada[4]
DMG MORI CO., LTD.
Nara, Nara, Japan
(yo-isaoka[3], yk-terada[4])@dmgmori.co.jp

***Abstract*—Machine tools are essential to the manufacturing industry, and the twin-drive stage, driven by two parallel-mounted motors, has recently been adopted to achieve higher precision in the system. However, this system generates a coupling force between the motors, which poses a significant challenge. Numerous advanced control strategies have been proposed to solve this issue, but they often introduce complexity and create difficulties for integration into the actual machine tools which only have limited controller architectures. This paper introduces an innovative method for transforming controllers from center-of-gravity (COG) to each axis coordination on the twin drive system. High-performance controllers originally designed for the COG coordination in the twin-drive system are adapted into individuaL-axis controllers using our proposed method. The effectiveness of the proposed method has been experimentally confirmed, achieving an 87.4% reduction in tracking error compared to the conventional method.**

***Index Terms*—equivalent controller transformation, mode decoupling, twin-drive machine tool stage**

I. Introduction

In recent years, the size of machine tools, illustrated in Fig. 1, has been increasing. Historically, single motors have been used to actuate the stages of these tools. However, to achieve a more accurate system, the concept of parallel twin-drive mechanisms, which employ two motors in tandem as shown in Fig. 2, has emerged. Consequently, numerous studies have been conducted to precisely control this system.

Generally, when operating machine tools, it is crucial to execute high-speed and high-precision control. Feedforward (FF) controllers are typically implemented to achieve high-speed performance, and many methodologies have been developed [1]–[3]. Conversely, to attain high-precision control, feedback (FB) controllers are the standard choice [4]–[6]. Consideration of nonlinear elements such as nonlinear friction and backlash is also considered to enhance control performance [7], [8]. However, the critical aspect of twin-drive system control lies in the management of the coupling force between the dual actuators, and the above research does not consider this point sufficiently.

Addressing the coupling force that affects control performance has been the focus of extensive research [10]–[14]. The study in [10] introduces self-resonance cancellation (SRC),

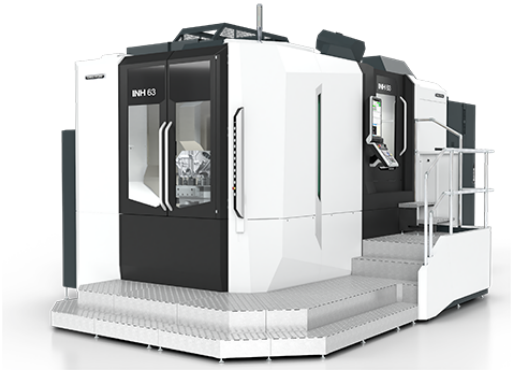

Fig. 1. Example of machine tool widely used in manufacturing [9].

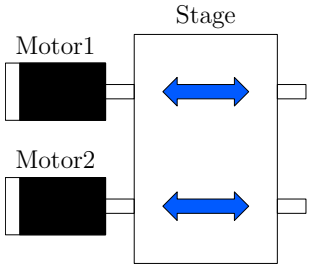

Fig. 2. System schematics of parallel twin-drive stage in machine tool.

enabling the independent design of resonance delegation and phase margin, though it does not account for dual actuators. The work in [11] suggests a decoupling control strategy for multiple actuators, but it concentrates on merging parallel and rotational modes rather than on identical plants of the twin-drive machine tool. In [12], a decoupling approach for parallel link type manipulators with equivalent mass matrices is presented, while [13] proposes a resonance suppression control technique utilizing virtual resistance, which could be informative for the twin-drive machine tool systems. The research in [14] develops a model-based FF controller for twin-drive rotary tables, presenting an interference and disturbance model applicable to FF control with genetic algorithm-based

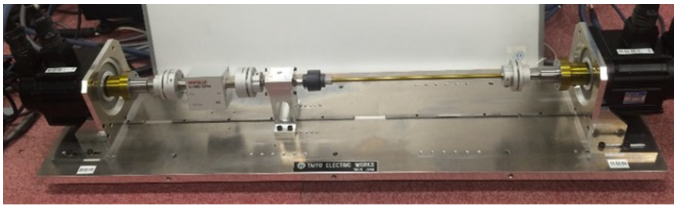

Fig. 3. Two-inertia system utilized for experimental validation of proposed method.

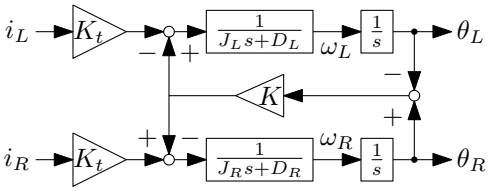

Fig. 4. Block diagram of two-inertia system.

parameter identification. While this solution demonstrates adequate fast-tracking performance, the methods tend to be too complex for practical implementation. Regarding this, a straightforward model-based decoupling control method has been recently proposed and validated for twin-drive two-inertia systems [15]. This method, which introduces virtual viscosity to transform the plant model, achieves both rapid and precise control performance; however, implementing this simpler controller in an actual industrial system can be even challenging due to the limitations of the software architectures where we can only adjust the PID gain in each axis controller.

Given these considerations, this paper introduces a controller conversion technique for actual machine tools based on the model-based decoupling approach in [15]. The method involves analyzing the control inputs from both FF and FB controllers and introducing equivalent controllers to replicate these control inputs in the actual system. The analytical part of this study focuses on a two-inertia system as fundamental research, and the validation of the proposed method is conducted through simulations and experiments.

The remainder of this paper is structured as follows: Section II details the problem setting. Section III presents the proposed method for controller conversion applicable to real-world industrial systems. Section IV validates the proposed method in the simulations. Section V describes experimental results to verify the benefits of the proposed method. Finally, Section VI concludes the paper and outlines prospective future research.

II. Problem Formulation

A. Modeling of two-inertia system

The goal of this research is to improve tracking performance in the twin-drive machine tool stage as shown in Fig. 2. As a fundamental study, this paper aims to control the center of mass position in the two-inertia system as shown in Fig. 3. The block diagram of the two-inertia system is shown in Fig. 4. i_R and i_L are the motor currents for the R-axis and L-axis, respectively. J_{R}, D_R, J_{L}, D_L, K, K_t are the inertia and

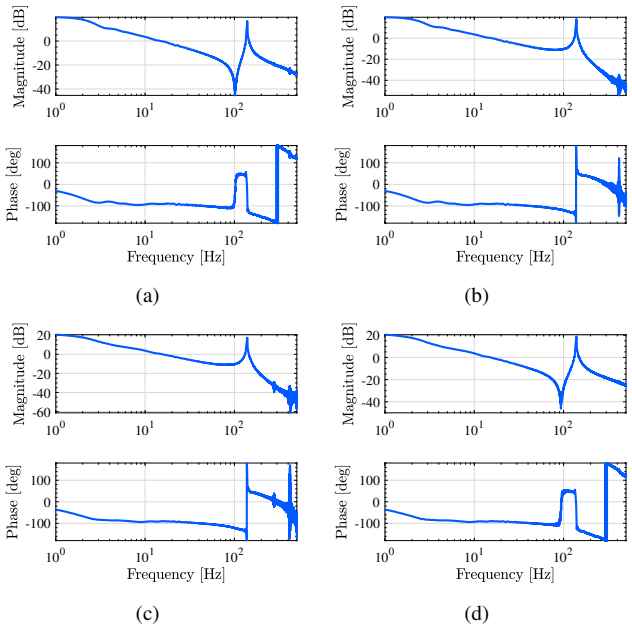

Fig. 5. Bode diagram of two-inertia system. (a) Right-side to right-side. (b) Right-side to left-side. (c) Left-side to right-side. (d) Left-side to left-side.

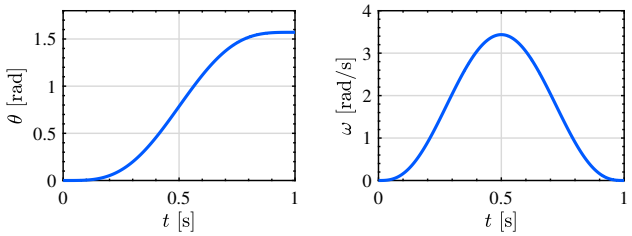

Fig. 6. Reference trajectory in experiments. (a) Position trajectory. (b) Velocity trajectory.

viscosity coefficients of the R-axis and L-axis motors, elastic coefficient, and motor torque coefficient, respectively. θ_R and θ_L are the angles of the R-axis and L-axis motors, respectively. ω_R and ω_L are the angular speeds of the R-axis and L-axis motors, respectively. The frequency response of the two-inertia system is shown in Fig. 5, and the parameters identified from the frequency response are listed in Table. I.

B. Mode decoupling to center-of-gravity coordinate with virtual viscosity

In this part, the mode decoupling method of the two-inertia system is presented based on [15]. The block diagram of the ideal control system is shown in Fig. 7. The mode decoupling is achieved by adding the virtual viscosity as shown in Fig. 7. Thanks to the virtual viscosity, motion equations of two-inertia system are decoupled from individual axes orientation to center-of-gravity (COG) orientation, which is detailed later. In this paper, the parallel mode of COG is called “sum mode”, and the rotational mode of COG is called “difference mode”. θ_{sum}, θ_{diff}, $\theta_{\mathrm{sum,ref}}$, $\theta_{\mathrm{diff,ref}}$, $\hat{\theta}_{\mathrm{sum}}$, $\hat{\theta}_{\mathrm{diff}}$ are the rotational angle

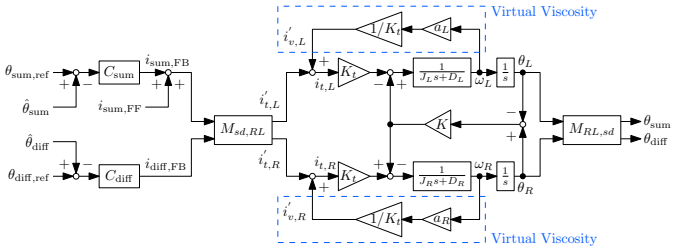

Fig. 7. Block diagram of ideal implementation.

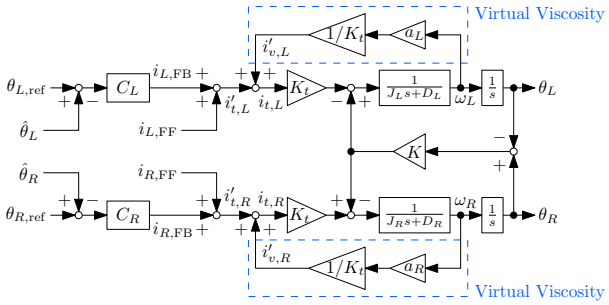

Fig. 8. Block diagram of actual implementation.

on the sum axis and diff axis, feedback reference of rotational angle to the sum mode controller and diff mode controller, and measured value of rotational angle on sum axis and diff axis, respectively. C_{sum} is the position controller for the sum mode, which is employed as a PID controller in this paper. C_{diff} is the position controller for the difference mode, which is employed as a P controller. $i_{\mathrm{sum,FF}}$, $i_{\mathrm{sum,FB}}$, $i_{\mathrm{diff,FB}}$ are the FF input for the sum mode controller, FB reference for the sum mode controller, and controller output of the sum mode controller, respectively. The FF input is generated within the framework of multirate FF control [1]. $i'_{t,R}$, $i'_{t,L}$, $i'_{v,R}$, $i'_{v,L}$, $i_{t,R}$, $i_{t,L}$ are the control inputs without virtual viscosity on the R-axis and L-axis, control inputs calculated as the virtual viscosity on the R-axis and L-axis, control inputs for the plants on the R-axis and L-axis, respectively. $M_{\mathrm{sd,RL}}$, $M_{\mathrm{RL,sd}}$ are the transform matrices from the COG modes to the individual axes and from the individual axes to the COG modes, respectively.

Considering only the control inputs $i'_{t,R}$, $i'_{t,L}$, without the virtual viscosity, the equations of motion on the two-inertia system as shown in Fig. 4 are given as,

$$J_R\frac{d^2\theta_R}{dt^2}+D_R\frac{d\theta_R}{dt}+K\left(\theta_R-\theta_L\right)=K_t i'_{t,R}, \tag{1a}$$
$$J_L\frac{d^2\theta_L}{dt^2}+D_L\frac{d\theta_L}{dt}+K\left(\theta_L-\theta_R\right)=K_t i'_{t,L}. \tag{1b}$$

We consider adding control inputs as the torques such as $K_t i'_{v,R}$, $K_t i'_{v,L}$ to the right-hand side of (1), respectively. Assuming that these control inputs are linear with respect to the rotational speed of individual axes motor, and considering the coefficients as a_R, a_L, we can express $K_t i'_{v,R}=a_R\frac{d\theta_R}{dt}$, $K_t i'_{v,L}=a_L\frac{d\theta_L}{dt}$. Then (1) becomes,

$$J_R\frac{d^2\theta_R}{dt^2}+\left(D_R-a_R\right)\frac{d\theta_R}{dt}+K\left(\theta_R-\theta_L\right)=K_t i'_{t,R}, \tag{2a}$$
$$J_L\frac{d^2\theta_L}{dt^2}+\left(D_L-a_L\right)\frac{d\theta_L}{dt}+K\left(\theta_L-\theta_R\right)=K_t i'_{t,L}. \tag{2b}$$

To convert (2) into the COG coordinate system, the below equations should be established:

$$\frac{D_R-a_R}{J_R}=\frac{D_L-a_L}{J_L}\left(=b\right). \tag{3}$$

In this paper, The condition $a_R=0$ is assumed. Then,

$$a_L=D_L-\frac{J_L}{J_R}D_R. \tag{4}$$

TABLE I
PARAMETERS OF TWO-INERTIA SYSTEM.

Parameter	Value
Right-side Motor Inertia J_R	$0.30\,\mathrm{mkgm}^2$
Right-side Motor Viscosity D_R	$3.0\,\mathrm{mNms/rad}$
Left-side Motor Inertia J_L	$0.24\,\mathrm{mkgm}^2$
Left-side Motor Viscosity D_L	$1.71\,\mathrm{mNms/rad}$
Torsional Rigidity K	$99.0\,\mathrm{Nm/rad}$
Motor Torque Coefficient K_t	$0.05\,\mathrm{Nm/A}$

Under (3) and (4), transforming (2) results in,

$$J_R\frac{d^2\theta_R}{dt^2}+bJ_R\frac{d\theta_R}{dt}+K\left(\theta_R-\theta_L\right)=K_t i'_R, \tag{5a}$$
$$J_L\frac{d^2\theta_L}{dt^2}+bJ_L\frac{d\theta_L}{dt}+K\left(\theta_L-\theta_R\right)=K_t i'_L. \tag{5b}$$

Regarding (5), if we sum up both sides of (5a) and (5b) and divide by J_R+J_L, or divide both sides of (5a) and (5b) by J_R and J_L respectively before subtracting them, the equations of motion expressed in sum and difference modes are,

$$\frac{d^2\theta_{\mathrm{sum}}}{dt^2}+b\frac{d\theta_{\mathrm{sum}}}{dt}=K_t i_{\mathrm{sum}}\,, \tag{6a}$$
$$\frac{d^2\theta_{\mathrm{diff}}}{dt^2}+b\frac{d\theta_{\mathrm{diff}}}{dt}+\left(\frac{K}{J_R}+\frac{K}{J_L}\right)\theta_{\mathrm{diff}}=K_t i_{\mathrm{diff}}. \tag{6b}$$

Here, i_{sum} and i_{diff} are expressed as,

$$\begin{bmatrix}\theta_{\mathrm{sum}}\\ \theta_{\mathrm{diff}}\end{bmatrix}=\begin{bmatrix}\frac{J_R}{J_R+J_L} & \frac{J_L}{J_R+J_L}\\ 1 & -1\end{bmatrix}\begin{bmatrix}\theta_R\\ \theta_L\end{bmatrix}=M_{\mathrm{RL,sd}}\begin{bmatrix}\theta_R\\ \theta_L\end{bmatrix}, \tag{7a}$$

$$\begin{bmatrix}i'_{t,R}\\ i'_{t,L}\end{bmatrix}=\begin{bmatrix}J_R & \frac{J_R J_L}{J_R+J_L}\\ J_L & -\frac{J_R J_L}{J_R+J_L}\end{bmatrix}\begin{bmatrix}i_{\mathrm{sum}}\\ i_{\mathrm{diff}}\end{bmatrix}=M_{\mathrm{sd,RL}}\begin{bmatrix}i_{\mathrm{sum}}\\ i_{\mathrm{diff}}\end{bmatrix}. \tag{7b}$$

Hence, the coupling system represented by (1) can be decoupled into non-coupling modes as shown in (6) by adding the virtual viscosity.

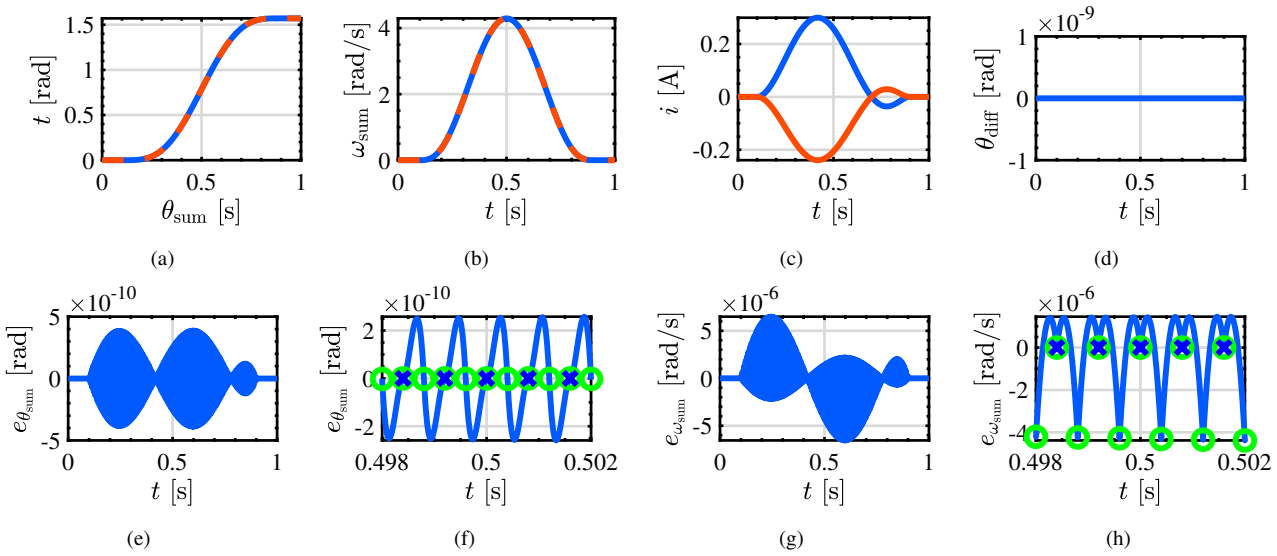

Fig. 9. Simulation results of proposed controller oriented at individual axes. (a) Center of gravity position. Reference value (—) and measured value (- · -). (b) Center of gravity velocity. Reference value (—) and measured value (- · -). (c) Control input. R-axis (—) and L-axis (—). (d) Difference position. (e) Position error. (f) Enlarged figure of position error. Circle marks for control period and cross marks for sampling period. (g) Velocity error. (h) Enlarged figure of velocity error. Circle marks for control period and cross marks for sampling period.

TABLE II
SIMULATION RESULTS REGARDING COULOMB FRICTION.

RMSE	Parameter Condition	θ Ideal [rad]	θ Prop. [rad]	θ Error Rate [%]	ω Ideal [rad/s]	ω Prop. [rad/s]	ω Error Rate [%]
w/o Coulomb	$d_R = 0, d_L = 0$	1.1334×10^{-12}	1.1334×10^{-12}	-5.7585×10^{-4}	2.7124×10^{-6}	2.7124×10^{-6}	-2.5338×10^{-7}
w/ Coulomb	$d_R = J_R d', d_L = J_L d'$	1.1164×10^{-4}	1.1164×10^{-4}	-1.9738×10^{-11}	4.4389×10^{-3}	4.4389×10^{-3}	-2.2528×10^{-11}
	$d_R = J_R d', d_L = 2J_L d'$	1.6169×10^{-4}	1.6169×10^{-4}	1.5842×10^{-3}	6.2596×10^{-3}	6.2597×10^{-3}	1.6799×10^{-3}
	$d_R = J_R d', d_L = 3J_L d'$	2.1168×10^{-4}	2.1170×10^{-4}	5.5889×10^{-3}	8.0022×10^{-3}	8.0027×10^{-3}	6.8812×10^{-3}

III. EQUIVALENT CONTROLLER TRANSFORM OF CENTER-OF-GRAVITY ORIENTED CONTROLLERS TO AXIS-SEPARATED COORDINATION

This section outlines the proposed method for converting the ideal controller, as illustrated in Fig. 7, into the practical controller depicted in Fig. 8. In Fig. 8, $\theta_{R,\mathrm{ref}}$, $\theta_{L,\mathrm{ref}}$, $\hat{\theta}_R$, $\hat{\theta}_L$ are the FB reference of rotational angle on the R-axis and L-axis, measured value of rotational angle on R-axis and L-axis, respectively. $i_{R,\mathrm{ref}}$, $i_{L,\mathrm{ref}}$, $i_{R,\mathrm{FB}}$, $i_{L,\mathrm{FB}}$ are the FF input for the R and L-axis controller, and FB reference for the R and L-axis controller, respectively. The ideal FF input $i_{\mathrm{sum,FF}}$ is transformed into $i_{\mathrm{R,FF}}$ and $i_{\mathrm{L,FF}}$, while the ideal feedback controllers C_{sum} and C_{diff} are converted into C_R and C_L, respectively.

The conversion of the FF input is executed based on (7b). The FF control input for the R-axis is set as $i_{\mathrm{R,FF}} = J_R i_{\mathrm{sum,FF}}$, and for the L-axis as $i_{\mathrm{L,FF}} = J_L i_{\mathrm{sum,FF}}$, assuming the FF input on difference axis $i_{\mathrm{diff,FF}} = 0$.

Next, the method for feedback controller conversion is described. Initially, the feedback controller inputs $i_{\mathrm{sum,FB}}$ and $i_{\mathrm{diff,FB}}$ are calculated as follows, utilizing (7a):

$$\begin{aligned} i_{\mathrm{sum,FB}} &= C_{\mathrm{sum}} \left(\theta_{\mathrm{sum,ref}} - \hat{\theta}_{\mathrm{sum}} \right), \\ &= C_{\mathrm{sum}} \cdot \frac{J_R}{J_R + J_L} \left(\theta_{R,\mathrm{ref}} - \hat{\theta}_R \right) \\ &\quad + C_{\mathrm{sum}} \cdot \frac{J_L}{J_R + J_L} \left(\theta_{L,\mathrm{ref}} - \hat{\theta}_L \right), \end{aligned} \tag{8a}$$

$$\begin{aligned} i_{\mathrm{diff,FB}} &= C_{\mathrm{diff}} \left(\theta_{\mathrm{diff,ref}} - \hat{\theta}_{\mathrm{diff}} \right), \\ &= C_{\mathrm{diff}} \left(\theta_{R,\mathrm{ref}} - \hat{\theta}_R \right) - C_{\mathrm{diff}} \left(\theta_{L,\mathrm{ref}} - \hat{\theta}_L \right). \end{aligned} \tag{8b}$$

From (7b) and (8), the feedback control input for the R-axis $i_{R,\mathrm{FB}}$ is computed as:

$$\begin{aligned} i_{R,\mathrm{FB}} &= \frac{J_R^2}{J_R + J_L} C_{\mathrm{sum}} e_{\theta_R} + \frac{J_R J_L}{J_R + J_L} C_{\mathrm{sum}} e_{\theta_L} \\ &\quad + \frac{J_R J_L}{J_R + J_L} C_{\mathrm{diff}} e_{\theta_R} - \frac{J_R J_L}{J_R + J_L} C_{\mathrm{diff}} e_{\theta_L}, \end{aligned} \tag{9}$$

where e_{θ_R} and e_{θ_L} are the position error on R-axis and L-axis, respectively. Assuming the condition where $e_{\theta_R} = e_{\theta_L}$, which establishes if $d_R = J_R d'$ and $d_L = J_L d'$ for the input disturbances d_R and d_L as d' is constant value (further

examined in the Appendix), $i_{R,\mathrm{FB}}$ simplifies to:

$$i_{R,\mathrm{FB}} = J_R C_{\mathrm{sum}} e_{\theta_R} \tag{10}$$

A similar approach is taken for the feedback control input for the L-axis $i_{L,\mathrm{FB}}$, yielding the equation:

$$i_{L,\mathrm{FB}} = J_L C_{\mathrm{sum}} e_{\theta_L} \tag{11}$$

Referring to (10) and (11), the feedback controller conversion is realized by setting $C_R = J_R C_{\mathrm{sum}}$ and $C_L = J_L C_{\mathrm{sum}}$.

IV. Simulation

To validate the proposed controller transforms, simulations are conducted on the two-inertia system as depicted in Fig. 4. In the simulations, the ideal controller as shown in Fig. 7 and the proposed controller as shown in Fig. 8 are implemented with the same poles in sum and difference modes. The simulation parameters are shown in Table. I.

The simulation results are presented in Fig. 9. In this paper, only the results from the proposed controller implementation are shown because it achieves perfect tracking performance as well as the ideal controller's results. Tracking errors of the rotational angle at COG are shown in Fig. 9(e), with a detailed view around $0.5\,\mathrm{s}$ provided in Fig. 9(f). The maximum tracking error is found to be less than the nano-order magnitude according to Fig. 9(e), achieving perfect tracking at each sampling period as shown in Fig. 9(f). Similar results are observed in the velocity performance as shown in Figs. 9(g) and 9(h). Fig. 9(d) shows the time response of the torsional angle θ_{diff}, as defined in (7a), maintaining $0\,\mathrm{deg}$. It signifies synchronized movement across both axes of the system.

The validity of the approximation as $d_R = J_R d'$ and $d_L = J_L d'$ in the proposed method is analyzed with coulomb friction, and the results are provided in Table. II. The coulomb friction is implemented as $J_R d' = 0.1\,\mathrm{A}$ in this simulation. The first column shows the results without coulomb friction, which means $d_R = 0\,\mathrm{A}, d_L = 0\,\mathrm{A}$. It indicates that error of the RMSE value in the rotational angle θ between ideal and proposed implementation differs only by the order of $10 \times 10^{-18}\,\mathrm{rad}$, which can be considered as a calculation error. When coulomb friction is included in the simulation, the same outcome occurs if $d_R = J_R d'$ and $d_L = J_L d'$, validating the approximation of the proposed method. It is also confirmed that the error between the ideal and proposed implementations increases if the condition where $d_R = J_R d'$ and $d_L = J_L d'$ is not established. These results show the validity of the approximation in the proposed method.

V. Experiments

This section presents the experimental results to validate the proposed method. The experiments are conducted for three approaches: each-axis-oriented controller without virtual viscosity as the conventional method; COG-oriented controller with virtual viscosity as the ideal method; and each-axis-oriented controller with virtual viscosity as the proposed method. These methods are applied to the two-inertia system shown in Fig. 3.

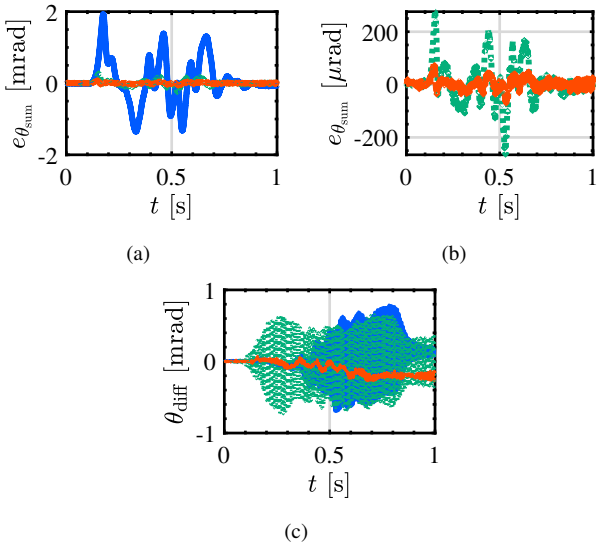

Fig. 10. Experimental results of conventional method (——), ideal implementation (- · -), and proposed actual implementation (····). (a) Error of rotational angle at COG. (b) Enlarged view of (a). (c) Torsional angle.

TABLE III
RMSE values obtained from experimental results.

	Conv.	Ideal	Prop.
Sum Position θ_{sum} [μrad]	590	20.5	74.6
Error Rate [%]	0	−96.5	−87.4

Each feedback controller design is conducted by pole placement using the parameters in Table. I. In the pole identification phase, it is increased by $50\,\mathrm{rad/s}$ from $100\,\mathrm{rad/s}$ until the torsional angle θ_{diff} is about to oscillate in the experiments. The proportional gain for C_{diff} is determined in the same way in the ideal implementation. Finally, the poles are determined as follows: $150\,\mathrm{rad/s}$ for C_R and C_L in the conventional method; $500\,\mathrm{rad/s}$ for C_{sum} and proportional gain $K_{\mathrm{p,diff}} = 10000$ for C_{diff} in the ideal method; $300\,\mathrm{rad/s}$ for C_{sum} converted into C_R and C_L in the proposed method.

Fig. 10 presents the experimental results. Fig. 10(a) depicts the tracking error of the rotational angle at the COG for the reference trajectory, as illustrated in Fig. 6(a). Although the controller architectures for both the conventional and proposed methods are identical other than the virtual viscosity, the proposed method demonstrates superior control performance. Fig. 10(b) provides an enlarged view of the tracking error shown in Fig. 10(a). This shows that the control performance of the ideal implementation surpasses that of the proposed method. This result seems to happen because there is the assumption in the proposed method that the same input disturbances occur on each axis. Table. III lists the RMSE values in the experiments. The error rate of the proposed method is improved by $87.4\,\%$ compared to the conventional method. These results indicate that the proposed method achieves a substantial enhancement over the conventional approach even if the controller architecture is limited.

VI. Conclusion

In this paper, we proposed a method that converts the ideal controllers into actual implementations for real machine tools. The controller transformation algorithm was derived from the analysis of the controller output. The effectiveness of the proposed method was verified through simulations and experiments using the two-inertia bench system, reducing the tracking error by $87.4\,\%$ compared to conventional methods.

In this study, the virtual viscosity was applied only to the L-axis. Future work will investigate the optimal distribution ratio of virtual viscosity for each axis. Disturbance analysis was not sufficiently conducted in this study, so future controller designs will be based on it to further improve the tracking performance in actual implementations. The final goal is to implement the proposed method in actual machine tools with a twin-drive mechanism, and further studies will be conducted in this regard.

Appendix A
Approximation analysis of rotational angle error

The frequency responses from the input disturbances d_R and d_L to the outputs θ_R and θ_L are analyzed in this section. The following relations for θ_R and θ_L are established:

$$\begin{aligned}\theta_R &= G_R\left(u_R - \tau_s + d_R\right),\\ &= G_R\left(-C_R\theta_R - K\left(\theta_R - \theta_L\right) + d_R\right), \qquad (12a)\\ \theta_L &= G_L\left(u_L + \tau_s + d_L\right),\\ &= G_L\left(-C_L\theta_L + K\left(\theta_R - \theta_L\right) + d_L\right), \qquad (12b)\end{aligned}$$

where u_R, u_L, and τ_s represent the control input on the R-axis, control input on the L-axis, and torsional torque, respectively. Deriving from equation (12), we obtain:

$$A = \begin{bmatrix} 1 + \left(C_R + K\right)G_R & -KG_R \\ -KG_L & 1 + \left(C_L + K\right)G_L \end{bmatrix}, \qquad (13a)$$

$$A\begin{bmatrix}\theta_R\\ \theta_L\end{bmatrix} = \begin{bmatrix} G_R d_R \\ G_L d_L \end{bmatrix}. \qquad (13b)$$

Exploiting (13), θ_R and θ_L are deduced as follows:

$$\theta_R = \frac{1}{|A|}\left[\left\{1 + \left(C_L + K\right)G_L\right\}d_R + KG_R d_L\right], \qquad (14a)$$

$$\theta_L = \frac{1}{|A|}\left[KG_L d_R + \left\{1 + \left(C_R + K\right)G_R\right\}d_L\right]. \qquad (14b)$$

where $|A|$ is the determinant of matrix A. In the parallel system depicted in Figure 2, the coulomb friction significantly impacts the tracking performance as the disturbance. Considering that the coulomb friction and inertia are both proportional to the mass, the input disturbances in the rotational system are defined as $d_R = J_R d'$ and $d_L = J_L d'$ as d' is a constant value. Considering (5) and (14) and $C_R = J_R C_{\mathrm{sum}}$, $C_L = J_L C_{\mathrm{sum}}$,

$$\begin{aligned}|A|(\theta_R - \theta_L) &= G_R d_R\left(1 + C_L G_L\right) - G_L d_L\left(1 + C_R G_R\right),\\ &= \frac{J_R d'}{J_R s^2 + bJ_R}\left(1 + \frac{J_L C_{\mathrm{sum}}}{J_L s^2 + bJ_L}\right),\\ &\quad - \frac{J_L d'}{J_L s^2 + bJ_L}\left(1 + \frac{J_R C_{\mathrm{sum}}}{J_R s^2 + bJ_R}\right) = 0.\end{aligned} \qquad (15)$$

Hence, the condition $e_{\theta_R} = e_{\theta_L}$ is established when $\theta_{\mathrm{R,ref}} = \theta_{\mathrm{L,ref}}$ and it is assumed that $d_R = J_R d'$ and $d_L = J_L d'$.

References

[1] H. Fujimoto, Y. Hori, and A. Kawamura, "Perfect Tracking Control Based on Multirate Feedforward Control with Generalized Sampling Periods," *IEEE Transactions of Industrial Electronics*, vol. 48, no. 3, pp. 636–644, 2001.

[2] M. Mae, W. Ohnishi, and H. Fujimoto, "MIMO multirate feedforward controller design with selection of input multiplicities and intersample behavior analysis," *Mechatronics*, vol. 71, pp. 1–9, 2020.

[3] M. Poot, J. Portegies, N. Mooren, M. van Haren, M. van Meer, and T. Oomen, "Gaussian Processes for Advanced Motion Control," *IEEJ Journal of Industry Applications*, vol. 11, no. 3, pp. 396–407, 2022.

[4] T. Kai, H. Sekiguchi, and H. Ikeda, "Control Structure with Dual Acceleration Feedback for Positioning Machine with Semi-Closed Servo System," *IEEJ Journal of Industry Applications*, vol. 11, no. 2, pp. 351–358, 2022.

[5] S. Yabui and T. Inoue, "Development of optimal controller design method to compensate for vibrations caused by unbalanced force in rotor system based on Nyquist diagram," *Journal of Vibration and Control*, vol. 25, no. 4, pp. 793–805, 2019.

[6] S. Yamada, K. Inukai, H. Fujimoto, K. Omata, Y. Takeda, and S. Makinouchi, "Proposal of Self Resonance Cancellation Control without Using Drive-Side Information," in *IEEE 41st Annual Conference of the IEEE Industrial Electronics Society (IECON)*, 2015.

[7] T. Hayashi, H. Fujimoto, Y. Isaoka, and Y. Terada, "Projection-based Iterative Learning Control for Ball-screw-driven Stage with Consideration of Rolling Friction Compensation," *IEEJ Transactions on Industry Applications*, vol. 9, no. 2, pp. 132–139, 2020.

[8] J. Padron, Y. Yokokura, K. Ohishi, T. Miyazaki, and Y. Kawai, "Evaluating the Equivalence between Nonlinear Friction and Backlash in Two-Inertia Systems," in *IEEE 17th International Conference on Advanced Motion Control (AMC)*, 2022.

[9] DMG MORI, "INH 63," https://www.dmgmori.co.jp/en/products/machine/id=6820, accessed: 2023-11-5.

[10] K. Sakata, H. Asaumi, K. Hirachi, K. Saiki, and H. Fujimoto, "Self Resonance Cancellation Techniques for a Two-Mass System and Its Application to a Large-Scale Stage," *IEEJ Journal of Industry Applications*, vol. 3, no. 6, pp. 455–462, 2014.

[11] W. Ohnishi, H. Fujimoto, K. Sakata, K. Suzuki, and K. Saiki, "Decoupling Control Method for High-Precision Stages using Multiple Actuators considering the Misalignment among the Actuation Point, Center of Gravity, and Center of Rotation," *IEEJ Journal of Industry Applications*, vol. 5, no. 2, pp. 141–147, 2016.

[12] K. Shimamoto and T. Murakami, "Force Sensorless Hybrid Position/-Force Control with Equivalent Mass Matrices Switching for Decoupled Rubbing Motion," *IEEJ Journal of Industry Applications*, vol. 12, no. 2, pp. 107–116, 2023.

[13] K. Natori, A. Ishikawa, and Y. Sato, "A Study on Resonance Suppression Control Based on Virtual Resistance Concept for Parallel Inverters in Islanded Microgrid," in *IEEE 9th International Power Electronics and Motion Control Conference (IPEMC2020-ECCE Asia)*, 2020.

[14] K. Ito, W. Maebashi, J. Ikeda, and M. Iwasaki, "Fast and Precise Positioning of Rotary Table Systems by Feedforward Disturbance Compensation Considering Interference Force," in *IEEE 37th Annual Conference of the IEEE Industrial Electronics Society (IECON)*, 2011.

[15] K. Fujimoto, H. Fujimoto, Y. Isaoka, and Y. Terada, "High Precision Control for Twin-Drive System of Machine Tool Based on Mode Decoupling with Virtual Viscosity: Basic Study on Two-Inertia System," in *IEE-Japan Technical Meeting on Mechatronics Control (PSS)*, 2023.